Spectrochimica Acta Part A: Molecular and Biomolecular Spectroscopy 101 (2013) 40–48

Contents lists available at SciVerse ScienceDirect

Spectrochimica Acta Part A: Molecular and Biomolecular Spectroscopy

journal homepage: www.elsevier.com/locate/saa

Raman spectroscopy of glyoxal oligomers in aqueous solutions

Elena Avzianova *, Sarah D. Brooks *

Department of Atmospheric Sciences, Texas A&M University College Station, TX 77843-3150, United States

HIGHLIGHTS

- Glyoxal oligomers in water droplets were studied by Raman and infrared spectroscopy.
- The interpretation of spectra was assisted by B3LYP calculations.
- Dihydrated glyoxal oligomers are formed in solutions with concentrations above 1 M.
- Both carbonyl groups of a glyoxal molecule are hydrated in aqueous solutions.
- Concentrated glyoxal droplets evaporate with incomplete water loss.

GRAPHICAL ABSTRACT

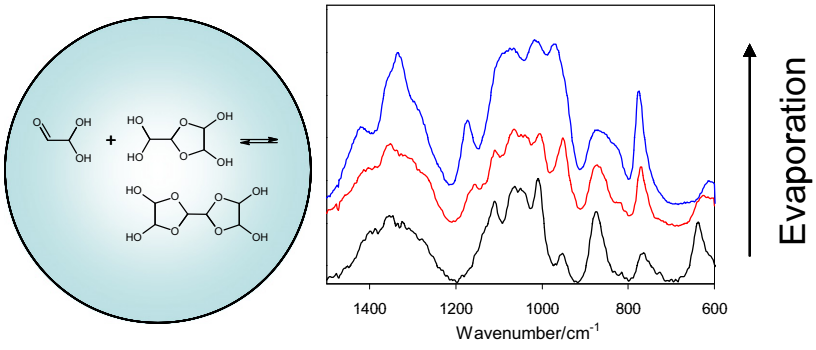

ARTICLE INFO

Article history:
Received 10 July 2012
Received in revised form 12 September 2012
Accepted 20 September 2012
Available online 3 October 2012

Keywords:
Glyoxal
SOA
Raman spectroscopy
FTIR
DFT

ABSTRACT

Raman microscopy and Attenuated Total Reflection infrared spectroscopy were utilized to facilitate investigations of equilibria between various hydrated and oligomeric forms of glyoxal in aqueous glyoxal solution droplets. The assignment of spectra is obtained with the assistance of B3LYP density functional quantum chemical calculations of vibrational wavenumbers, Raman activities, and infrared intensities. Several forms of glyoxal derivatives with similar functional groups, e.g., hydroxyl and dioxolane rings, are found to be present. The absence of a Raman spectral peak corresponding to the vibrational carbonyl stretch provides evidence that both carbonyl groups of a glyoxal molecule become hydrated in solutions of a broad concentration range. The presence of bands corresponding to deformation vibrations of the dioxolane ring indicates that dihydrated glyoxal oligomers are formed in glyoxal solutions with concentrations of 1 M and higher. Under typical ambient temperature and humidity conditions, concentrated glyoxal solution droplets undergo evaporation with incomplete water loss. Our results suggest that formation of crystalline glyoxal trimer dihydrate from concentrated solutions droplets is hindered by the high viscosity of the amorphous trimer and requires dry conditions that could rarely be achieved in the atmosphere. However, crystallization may be possible for droplets of low initial glyoxal concentrations, such as those produced by evaporating cloud droplets.

Introduction

Glyoxal is produced in high yields in the atmosphere by the oxidation of aromatic hydrocarbons and in smaller yields by reactions of isoprene and terpenes [1–4]. Gas phase glyoxal molecules can be scavenged by cloud droplets and fog. In the condensed phase, these molecules are hydrated and involved in self-reactions to form acetal oligomers [5]. Measured concentrations of glyoxal in solution exceed concentrations predicted by Henry's law [6,7]. The discrepancy may be driven in part by the accessibility of water, since glyoxal forms hydrated species in solution, allowing higher solubility of glyoxal than expected [6]. Furthermore, hydrogen bonding within single glyoxal oligomers and between two oligomers and water molecules may provide stabilization of condensed phase products.

Quantifying the formation of secondary organic aerosol (SOA) products in evaporating cloud droplets is a challenge, since

* Corresponding authors.
E-mail addresses: eavzianova@tamu.edu (E. Avzianova), sbrooks@tamu.edu (S.D. Brooks).

1386-1425/$ - see front matter © 2012 Elsevier B.V. All rights reserved.
http://dx.doi.org/10.1016/j.saa.2012.09.050

reactions occurring in a water-restricted environment do not necessarily proceed by the same mechanisms as those which occur when water is readily available. Furthermore, products may depend on concentrations of organic compounds and rates of evaporation. Non-volatile products of SOA reactions remain in the condensed phase after cloud droplets evaporate [8,9]. Condensed phase product identification and yields for reactions involving aldehydes, ketones, and organic acids are important for assessing the contribution of heterogeneous organic chemistry to total atmospheric aerosol loadings and thus, the anthropogenic and biogenic aerosol impacts on clouds and climate.

Availability of water plays a key role in the glyoxal chemistry, as illustrated by Reaction (1a) and (1b). In aqueous solution, one or both aldehyde groups of the glyoxal can become hydrated [10].

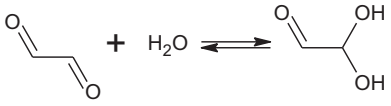

(1a)

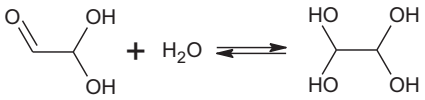

(1b)

Two monohydrates can then react through nucleophilic attack of an OH group on the reactive carbonyl of the neighboring molecule (Reaction (2)).

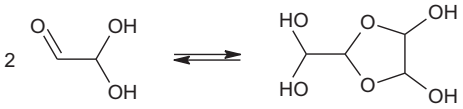

(2)

NMR data suggests that the majority of glyoxal dimers structures are most likely linked via five-membered 1,3-dioxalane rings [11–13]. If the gem–diol formed in Reaction (2) becomes dehydrated, it can then react with a third glyoxal monohydrate, forming the stable glyoxal trimer (which contains two dioxolane rings) (Reaction (3)). According to calculations, the trimer is the thermodynamic sink among all glyoxal derivatives involved in these reactions [14].

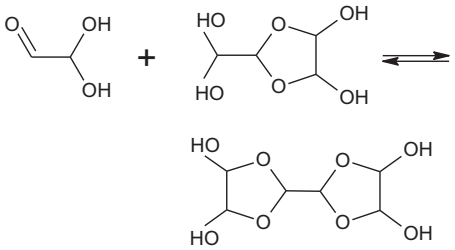

(3)

While it has been observed in our laboratory and others that while oligomers form in low yields in dilute solutions, yields appear to be increased by evaporation at low relative humidities [15]. Such observations may be justified by the fact that the dihydrate (formed in Reaction (1)) lacks the carbonyl group required for the self-reactions and cannot react as monohydrates do (as shown in Reactions (2) and (3)). Furthermore, water may play a significant role in formation of amorphous solids, in which increased hydrogen bonding and increased viscosity limit crystallization [5]. Understanding the water-mediated equilibria of reactions of aldehydes, ketones and other organic compounds is important for assessments of the chemical and physical properties of atmospheric aerosols [16,17].

Spectroscopic studies in water-restricted environments may provide insight into how water availability impacts the products and yields of reactions of organic compounds in cloud droplets and the resulting aerosol phase. From this point of view it is important to determine the assignments of vibrations in Raman spectra of glyoxal and its derivatives formed in water solutions under different conditions. Accurate peak assignments may be used to monitor modifications of the structure by the environment when physical factors such as temperature and water availability are varied. Previous spectroscopic investigations of glyoxal oligomers in aqueous solutions have focused on infrared (IR) spectroscopy [10,18], in which assignment of the glyoxal spectral features is complicated by interferences from water, which is a strong absorber in the infrared. Since water shows low Raman activity, Raman spectroscopy may be very suitable for investigation of equilibria in glyoxal aqueous solutions. To the best of our knowledge Raman spectra have been reported only for anhydrous glyoxal monomer (CHOCHO) in liquid [19] and solid [20] phases, including polycrystalline glyoxal in N_2-glyoxal matrix frozen at 5 K [21]. Also, photoacoustic Raman spectroscopy (PARS) and Coherent anti-Stokes Raman spectroscopy (CARS) have been used to study glyoxal in the vapor phase [22]. In order to fill the existing gap, we have recorded Raman spectra of glyoxal solutions of different concentrations in water and deuterated water (D_2O). The interpretation of the spectra is supported by theoretical computations of vibrational wavenumbers and Raman intensities obtained using Electronic Structure Density Functional Theory (DFT).

Experimental

Materials and methods

Solutions of glyoxal monomer dihydrate were prepared by hydrolyzing glyoxal trimer dihydrate (GTD) powder (92%, ICN Biomedicals, Inc.) in deionized water (18 Ω cm^{-1}) overnight, followed by dilution with additional water. The concentrations of glyoxal solutions varied from 0.1 M to 4.0 M. Deuterated water (99.9 atom% D, Aldrich) was used for preparation of the D_2O solutions.

To examine the effect of glyoxal oligomerization on solution composition, evaporation experiments were performed. To begin an experiment, a 20–30 μl glyoxal solution droplet was placed on the aluminum foil and exposed to the air. Drying experiments were repeated using a range of droplet solution concentrations of 1.0–4.0 M. An additional series of experiments was conducted using deuterated water in place of the H_2O. To eliminate exchange with water molecules of air, evaporation of glyoxal solutions in D_2O droplets was conducted in a dessicator with silica gel.

Upon evaporation, aqueous concentrated glyoxal solutions leave behind a thicker film than dilute solutions. The crystallization behavior is likely caused by hindered transport of water in highly viscous amorphous material. In order to remove the remainder of water from amorphous glyoxal obtained from concentrated solutions, the samples were placed in a dessicator with silica gel overnight.

Raman spectroscopy

Raman spectra were recorded over the range of 500–3500 cm^{-1} using a Thermo Fisher Scientific DXR Raman Spectrometer, equipped with an Olympus BX microscope and a high resolution CCD detector. A frequency doubled Nd:YVO_4 diode pumped solid state laser was used for excitation at 532 nm. The Raman apparatus also features a motorized stage that moves automatically in the *x* and *y* directions to image areas multiple areas within a single droplet. Raman spectra of glyoxal solutions in H_2O and D_2O in the range of concentration between 1 and 4 M were recorded.

Infrared spectroscopy

In addition to the Raman measurement, Fourier Transform Infrared Spectroscopy (FTIR) spectrum of aqueous glyoxal solutions were recorded in the region between 2000 and 700 cm^{-1} using a Nicolet Magna 560 spectrometer equipped with an Attenuated Reflectance (ATR) cell and an MCT detector for a subset of solutions droplets. Standard spectra of solid glyoxal trimer dihydrate were recorded by pressing crystals onto the ZnSe crystal of the ATR (Pike Technologies). Standard glyoxal solution spectra were taken using the same conditions as the Raman spectra but with a water droplet as the background and without any evaporation delays.

Calculations

Density Functional Theory (DFT) calculations were performed using Gaussian 03 at the B3LYP/6-311 + G(d,p) level of theory, using an ultrafine pruned grid and tight optimization criteria [23]. Geometry optimization, Raman shift (wavenumber), and Raman scattering activity calculations were completed for mono- and di-hydrated glyoxal monomer, mono- and di-hydrated dimers of glyoxal, trimer glyoxal dihydrate, and their OD analogues. The B3LYP method is less computationally expensive than traditional correlated *ab initio* methods while providing a comparable accuracy in computing structural properties of large molecules, including molecular geometry and vibrational wavenumbers [24]. The theoretical Raman intensities I_i^R were calculated based on the Raman scattering activities S_i obtained from the Gaussian program according to Eq. (1) [25],

$$I_i^R = C \cdot (v_0 - v_i)^4 \cdot v_i^{-1} \cdot B_i^{-1} \cdot S_i \quad (1)$$

$$B_i = 1 - \exp(-hv_i c/kT) \quad (2)$$

where C is a constant (10^{-12}), is the B_i is the temperature factor which accounts for the intensity contribution of excited vibrational states (Eq. (2)), ν_0 is the laser excitation frequency, ν_i is the frequency of normal mode, k is the Boltzman constant, c is the speed of light, h is the Planck constant, and T is the temperature.

Results and discussion

Fig. 1 shows Raman spectra of aqueous solutions, ranging from 1.0 to 4.0 M aqueous glyoxal, and crystalline glyoxal trimer. In this concentration range, spectra have very similar features with a few minor differences as discussed below. The largest differences are observed between spectra of glyoxal solutions and crystalline glyoxal dihydrate timer. Evaporation under ambient conditions required extended periods of time and lead to the formation of highly viscous, amorphous glass-like material. The Raman spectrum of amorphous glyoxal contains traces of water and is very close to the spectrum of crystalline glyoxal trimer. Results of the droplet drying experiments depended on solution concentration. The spectra of initially 1 M glyoxal under evaporation are shown in Fig. 2. Drying of glyoxal obtained from more dilute solutions (initial concentrations lower than 0.5 M) resulted in solidification of crystalline glyoxal trimer.

To facilitate assignment of glyoxal derivatives, spectra of glyoxal solutions in D_2O were also obtained (Fig. 3). Also FTIR spectra of crystalline glyoxal dihydrate trimer and glyoxal solutions in the range of concentration between 1.0 and 4.0 M were recorded, as shown in Fig. 4.

To complete the vibrational assignments of the experimental spectra of glyoxal derivatives, quantum chemical calculations were performed for the following forms of glyoxal and its deuterated analogues:

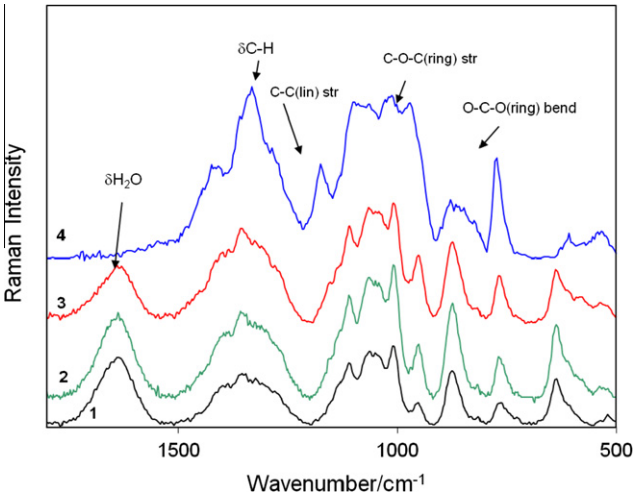

Fig. 1. Raman spectra of 1–4 M glyoxal solutions in the 1800–500 cm^{-1} region. Black line (1): 1 M glyoxal solution. Green line (2): 2 M glyoxal solution. Red line (3): 4 M glyoxal solution. Blue line (4): crystalline glyoxal trimer. (For interpretation of the references to color in this figure legend, the reader is referred to the web version of this article.)

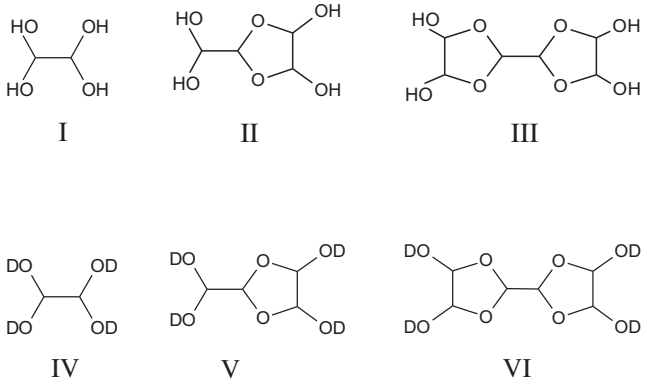

The structures were optimized at the B3LYP/6-311 + G(d,p) level of theory. The resulting geometries and wave functions corresponding to energy minimum were used in the normal coordinate analysis, as implemented in Gaussian, to calculate wavenumbers and Raman activities. A relatively large basis set was used to obtain accurate structural parameters and vibrational wavenumbers. Since Raman intensities are known to be sensitive to diffuse augmentation of the basis set, diffuse functions were used in all calculations [26]. For instance, the systematic study reported by Cheeseman and Frisch [27] showed that Raman Optical Activity tensor invariants require basis sets with diffuse functions to obtain reliable Raman activities. Calculated wavenumbers and Raman activities with experimental data for hydrated/deuterated glyoxal derivatives and water/deuterated water solutions are presented in Tables 1 and 2. Optimized structures and corresponding Cartesian coordinates of all derivatives are now provided in Supplementary Information (Figs. S1–S3 and Tables S1–S3). Comparison of calculated spectra of glyoxal derivatives with experimental spectra of glyoxal solutions and glyoxal crystalline trimer dihydrate shows general qualitative agreement between the Raman intensities (Fig. 5).

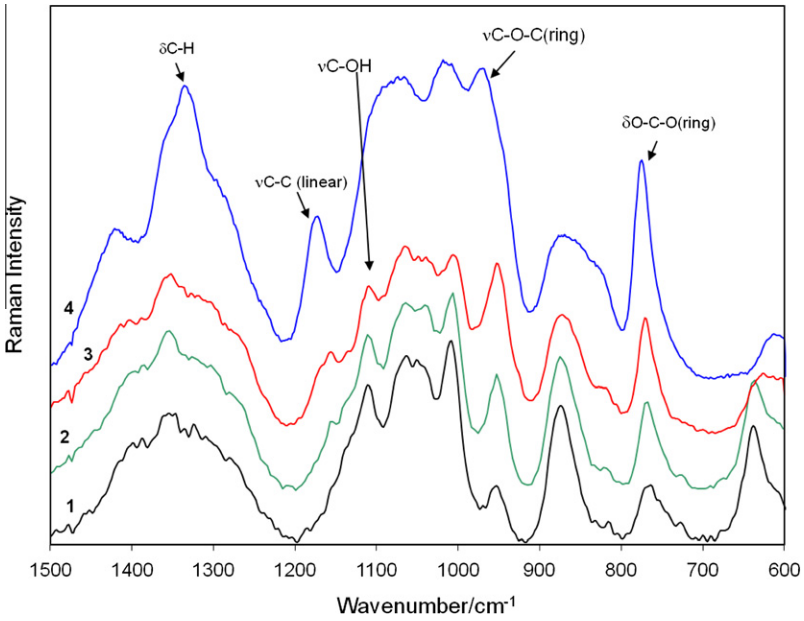

Fig. 2. Raman spectra of glyoxal solutions upon evaporation. Black line (1): 1 M glyoxal solution. Green line (2): 1 M glyoxal solution after 20 min exposure on air. Red line (3): 1 M glyoxal solution after 1 h exposure on air. Blue line (4): crystalline glyoxal obtained over silica gel. (For interpretation of the references to color in this figure legend, the reader is referred to the web version of this article.)

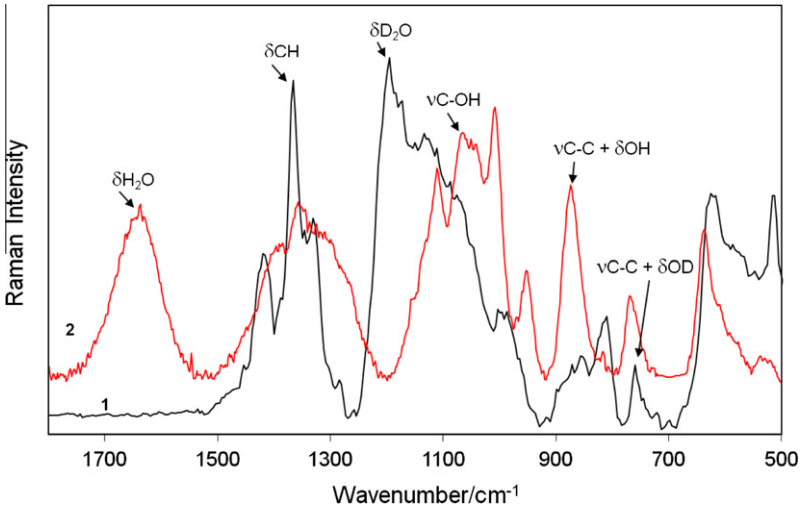

Fig. 3. Raman spectra of glyoxal solution in the 1600–600 cm^{-1} region. Black line (1): 2 M glyoxal solution in D2O. Red line (2): 2 M glyoxal solution. (For interpretation of the references to color in this figure legend, the reader is referred to the web version of this article.)

The primary difference between the spectra of glyoxal solutions and that of crystalline glyoxal trimer is the water peak at 1640 cm^{-1} (Fig. 1). During evaporation of glyoxal aqueous solutions, the intensity of the 1640 cm^{-1} band decreases significantly due to water removal (Fig. 1). The drying is also accompanied by changing intensities and shifting of bands in the region of C—C and C—O stretching and C—H deformation of glyoxal derivatives (1200–700 cm^{-1}). The spectra of heavy water glyoxal solutions show the same behavior upon evaporation as H_2O glyoxal solutions, except that the scissoring bend of D_2O lies in the region at 1200 cm^{-1} [28], overlapping the C—C and C—O stretching region (Fig. 3). Significant differences between spectra of aqueous and heavy water glyoxal solutions appear mainly in spectral regions around 1400–1300 and 1200–1000 cm^{-1} (Fig. 3). Below we provide detailed assignments of Raman features in several spectral regions.

Region 1500–1100 cm^{-1}. C—H bending vibrations occur in the region 1400–1450 cm^{-1} and C—H twisting vibrations give rise to a band around 1300–1390 cm^{-1} (Fig. 1) [29]. It is known that the frequency of C—H deformations are often very sensitive to the degree of vibrational coupling with other coordinate displacements. The C—H bending vibration involves a large displacement of the carbon atom, which couples with adjacent C—C stretching vibration, leading to splitting the C—H bending bands. In glyoxal dihydrates, C—H deformation vibrations extensively mix with C—C stretching and δO—H in-plane deformation, resulting in massive envelope of bands. In the spectra of solid glyoxal trimer in both amorphous and crystalline forms this spectral feature has an intensity maximum at 1330 cm^{-1}, whereas in liquid glyoxal solutions the intensity maximum is shifted to 1353 cm^{-1} (Fig. 2). According to our calculations the spectral feature at 1353 cm^{-1} is attributed to C—H bending of monomer and dimer glyoxal gem–diol group

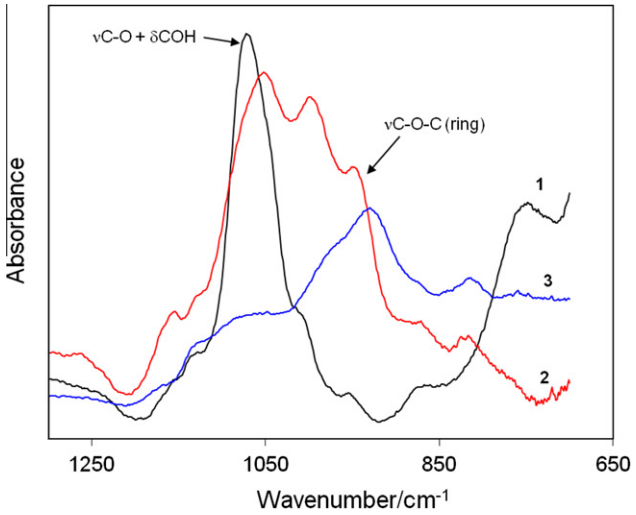

Fig. 4. FTIR spectra of glyoxal solutions upon evaporation. Black line (1): 1 M glyoxal solution. Red line (2): 4 M glyoxal solution. Blue line (3): crystalline glyoxal obtained over silica gel. (For interpretation of the references to color in this figure legend, the reader is referred to the web version of this article.)

(Table 1). Features at lower frequencies are assigned to C—H deformation vibrations of the dioxolan ring. A band at 1340 cm^{-1} is common for lone C—H bending [30]. For instance, in-plane methyne C—H bending band for 2-propanol and its deuterated analogues occur at 1340 cm^{-1} [31]. Spectra of both liquid glyoxal solution and solid glyoxal have additional features at 1425 and 1280 cm^{-1}. After evaporation these features become more evident on both sides of the envelope of bands (Fig. 2). These bands are attributed to the C—H bending mode coupled with different O—H deformation modes. Anderson and Bellamy [32] have studied the spectra of gem–dihydroxy compounds produced by hydration of carbonyl group and reported a similar splitting of C—H bending bands. They showed that upon hydration aldehydic C—H deformation mode that occurs in the region of 1350–1370 cm^{-1} disappears and is replaced by a doublet at 1440–1420 and 1450–1410 cm^{-1} and another peak at 1290–1280 cm^{-1} due to coupling two different δOH with adjacent C—H bending, confirming our assignment.

In glyoxal solutions in deuterated water, the corresponding δOD vibration modes shifted to lower frequency and simplifying this spectral region (Fig. 3). Due to decoupling of vibrations, the spectrum of deuterated glyoxal solution shows a distinct maximum at 1368 cm^{-1} corresponding to C—H wagging of monomer glyoxal, in a good agreement with calculated wavenumber 1370 cm^{-1} for this mode (Table 2). The distinct band at 1423 cm^{-1} (Fig. 3) in this spectra corresponds to a vibration mode containing a high degree of C—H bending related to gem–diol group as well as O—CH bending of dioxolane ring.

Region 1200–1100 cm^{-1}. C—OH stretching vibrations occur in the region of 1000–1200 cm^{-1} [29,33], giving rise to considerable overlapping with C—C stretching vibration bands. Spectra of solid glyoxal trimer shows band with medium intensity at 1175 cm^{-1} (Fig. 1) assigned to linear C—C stretching mode with adjacent dioxolane rings of glyoxal trimer mixed with C—H bending motion, which is in a good agreement with predicted value of 1177 cm^{-1}

Table 1
Calculated wavenumbers and Raman activities of glyoxal derivatives.

Calculated						Observed		Assignment
I		II		III		1 M (H_2O)[a]	Solid[b]	
ν, cm^{-1}	RA	ν, cm^{-1}	RA	ν, cm^{-1}	ν, RA	ν, cm^{-1}	ν, cm^{-1}	
589	3					639	610	
761	1.1	758	1.1			762		$OCO_{bending}$ (monomer)
				775	5.8		770	$OCO_{bending}$ (ring)
		823	2.4	816	3.4	817	819	
853	7					872		nC—C (mono-,dimer) + dOH
		879	11				879	
		953	6.4	954	14.5	952		ring stretching
		974	1.7	982	2.4	970.7	972	nC—O—C (r) + dC—C (linkage)
				1001	17.8			
		1007	3.4			1008	1002	
1018	6			1024	1.6		1012	
1050	4	1050	1.5			1042	1027	nC—O + C—OH_{bend} ip
				1060	10.6			
		1068	4.1	1069	7.8	1065	1066	
1089	5	1082	2				1099	nC—OH
1110	2	1103	5	1102	3.1			
		1159	1			1110		nC—OH (gem–diol)
				1177	2.2	1155 sh	1160	nC—$C_{linkage}$ (dimer) + ring str
1185	1						1174	nC—$C_{linkage}$ (trimer)
		1204	1.1	1203	1.2			
		1223	2					
		1230	5	1234	8	1278	1283	CH_{bend} + OH_{bend}
1258	5							
1280	6	1296	2.5					
				1324	5			
1338	3	1332	3				1334	C—H_{bend} (ring)
		1365	3.3	1366	10	1353		C—H_{bend} (monomer, dimer)
1376	4	1370	3.3	1379	3.4			
		1377	3.7	1393	6			
1402	3	1414	1.1				1421	CH_{bend} + OH_{bend}
1430	3			1436	3.6			
1465	2	1462	1					
		1473	2.6	1469	2.8			

[a] 1 M aqueous glyoxal solution.
[b] Crystalline glyoxal trimer.

for this mode. In aqueous glyoxal solutions with concentrations from 0.5 to 1 M, no distinct bands are observable near this wavenumber, possibly due to interference by the strong band at 1110 cm^{-1} which is assigned to C—OH stretching mode of gem–diol group of dihydrated glyoxal. However, with increasing concentration solution, a new peak at 1155 cm^{-1} and a shoulder at 1175 cm^{-1} arise. The band at 1155 cm^{-1} is assigned to linear C—C linkage stretching vibration coupling with ring stretching deformation in dihydrated glyoxal dimer. After transition to solid state, the peak at 1155 cm^{-1} disappears and the 1175 cm^{-1} feature takes its place.

During evaporation, the band at 1110 cm^{-1} is overlaid by a strong band near 1099 cm^{-1}. According to calculations, C—O stretching of the gem–diol glyoxal derivative appears at 1110 and 1103 cm^{-1} for dihydrated monomer and dimer glyoxal, respectively. For deuterated analogues, the corresponding predicted wavenumbers shift to 1130 and 1136 cm^{-1} for the monomer and dimer, respectively (Table 2 and Fig. 3). A similar blue shift of C—O stretching vibration bands has been observed in IR spectra of lactic acid and lactate where two bands at 1125 and 1090 cm^{-1}, assigned to the νC—O modes of the two forms, associated and free OH, move to 1160 and 1100 cm^{-1} on deuteration [34]. Also in the spectra of 1,1,1-trifluoro-2-propanol the νC—O band has been shown to shift from 1060 to 1110–1130 cm^{-1} on hydroxyl group deuteration [31].

The water O–D deformation vibration band at 1200 cm^{-1} appears in the spectrum of deuterated water glyoxal solution coupling with linear C—O and C—C linkage stretching modes in the 1155–1180 cm^{-1} area and overlapping the region. Spectra of deuterated glyoxal solution show an aggregate of unresolved bands with spectral features at 1180, 1138, 1112 and 1090 cm^{-1} (Fig. 3). According to our calculation, the band at 1180 cm^{-1} is attributed to the νC—C linear linkage of deuterated glyoxal dimer hydrate with a theoretical wavenumber of 1183 cm^{-1}. The predicted value for νC—O of gem–hydroxyl groups coupling with δCH is 1136 and 1129 cm^{-1} in deuterated glyoxal monomer hydrate and dimer hydrate, respectively (Table 2). Based on our calculations, we assigned the band with wavenumber 1138 cm^{-1} to a νC—O of gem–diol. A band at 1112 cm^{-1} is assigned to a νC—O of hydroxyl groups connected to dioxolane ring of glyoxal dimer dideuterate, in a good agreement with predicted wavenumber of 1113 cm^{-1} for this vibration mode. Unresolved peaks of lower intensity at 1092 cm^{-1} likely correspond to the νC—O of OD groups connected to dioxolane ring of glyoxal trimer dideuterate. The calculated wavenumber for this vibration mode is 1081 cm^{-1}.

Region 1100–900 cm^{-1}. In the region between 1000 and 1100 cm^{-1} spectra of aqueous glyoxal solutions feature a strong broad band with peaks at 1062, 1050 and 1007 cm^{-1} (Fig. 1). This group of peaks are predominantly a C—O stretching mode mixed with C—OH in-plane bending. The theoretical wavenumber for the C—O stretching mode of hydroxyl groups connected to dioxolane ring of glyoxal dimer is 1068 cm^{-1} (Table 1). For glyoxal solution concentration of 1 M and higher, a medium band appears with wavenumber 952 cm^{-1}. The of this band increased with increasing of glyoxal concentration. Raman spectra of dimethyl substituted 1,3-dioxolanes show weak to medium bands at 955–947 cm^{-1} due to ring breathing vibration [35,36]. In theory, there are Raman-active vibrations are present at 953 and 954 cm^{-1} for

Table 2
Observed and calculated wavenumbers and Raman activities of deuterated glyoxal derivatives.

Calculated						Observed		Assignment
IV		V		VI		2 M (D_2O)[a]	Solid[b]	
ν, cm^{-1}	RA	ν, cm^{-1}	RA	ν, cm^{-1}	RA	ν, cm^{-1}	ν, cm^{-1}	
554	2	537	5	615	4	629	609	
793	5	748	2	764	8	762		$OCO_{bending}$ (monomer)
							770	$OCO_{bending}$ (ring)
		809	3	804	3	814	818	
		841	5	835	5			
865	4	859	5			865	865	nC—C
907	5	918.6	2			875	883	
		941	3	939	2			
969	4	968	2				972	
		983	5	984	10	989	989	ring stretch + dOD
				994	15	997		
1008	2					1003		
				1028	1			
		1044	2	1044	12		1041	
1057	3	1064	5					
				1081	3	1092		$nC—OD_{ring}$ (trimer)
				1102	3		1101	
		1113	2	1113	6	1112		$nC—OD_{ring}$ (dimer)
							1119	
1129	2	1136	2			1138		nC—OD (monomer)
							1172	
		1183	3	1186	4	1180		$nC—C_{linkage}$ (dimer)
1201	4					1200		
						1286	1297	
		1315	4	1308	7			
		1345	2			1331	1331	
		1352	5					
1361	6	1358	3	1355	10		1357	
1370	7					1368		$C—H_{wagging}$ (monomer)
		1380	3	1385	3			
1404	1							
1423	2	1423	3	1424	2	1423	1423	CH_{bend} + OCH_{bend} (ring)
				1446	6			

[a] 2 M glyoxal solution in heavy water.
[b] Crystalline glyoxal trimer obtained after evaporation of heavy water solution.

dihydrated glyoxal dimer and dihydrated glyoxal trimer, respectively (Table 1). Neither theoretical, nor experimental spectra of glyoxal monomer (CHOCHO) [21,22] show absorbance in this area. According to this, we assign the band at 950 cm^{-1} to ring stretching and conclude that the cyclic dihydrated glyoxal dimer is present in detectable concentration even in 1 M solution.

In spectra of deuterated glyoxal solutions, the band at 952 cm^{-1} is absent because the band corresponding to ring stretching in O–D derivative of the dihydrated glyoxal dimer is shifted to a higher wavenumber. A theoretical prediction for this vibration mode is 983 cm^{-1} (Table 2). As shown in Fig. 4, experimental spectra of deuterated glyoxal solutions have several bands in the region between 960 and 1010 cm^{-1} that originate from ring stretching and in-plane OD bending (δOD). Indeed, in long-chain alcohols, the δOD peak appears at about 940 cm^{-1} with an intensity ranging from moderate to weak [37]. In deuterated gem–diols, a doublet corresponding to δOD appears at two regions from 905 to 930 and from 913 to 966 cm^{-1} [32].

Upon transition to the crystalline form of glyoxal trimer dihydrate, the intensity of a band at 950 cm^{-1} decreases and the band overlaps with a new strong band at 972 cm^{-1} (Fig. 2). According to our calculations, this new band could be assigned to C—O—C stretching of rings involving bending of C—C linkage between two dioxolane rings vibration mode, which has a predicted wavenumber of 982 cm^{-1}.

Region 900–800 cm^{-1}. In the 900–800 cm^{-1} region spectra of water glyoxal solution feature the strong peak at 872 cm^{-1} (Fig. 1). During evaporation, the intensity of this peak decreases significantly and new peaks of lower intensity appear, overlapping over peak in this region. Resulting spectrum of crystalline glyoxal shows few overlapping peaks of low intensity between 820 and 880 cm^{-1}. In contrast, the spectrum of deuterated glyoxal solution contains a massive band with two distinct maxima at 875 and 865 cm^{-1} and also a new medium-intensity feature containing several overlapping bands with a maximum intensity at 814 cm^{-1} (Fig. 3). Upon evaporation, the band at 814 cm^{-1} disappears and the intensity of the peak at 865 cm^{-1} increases. The absence of a strong 872 cm^{-1} band in deuterated solutions suggests that this vibration mode is be affected by OH motion.

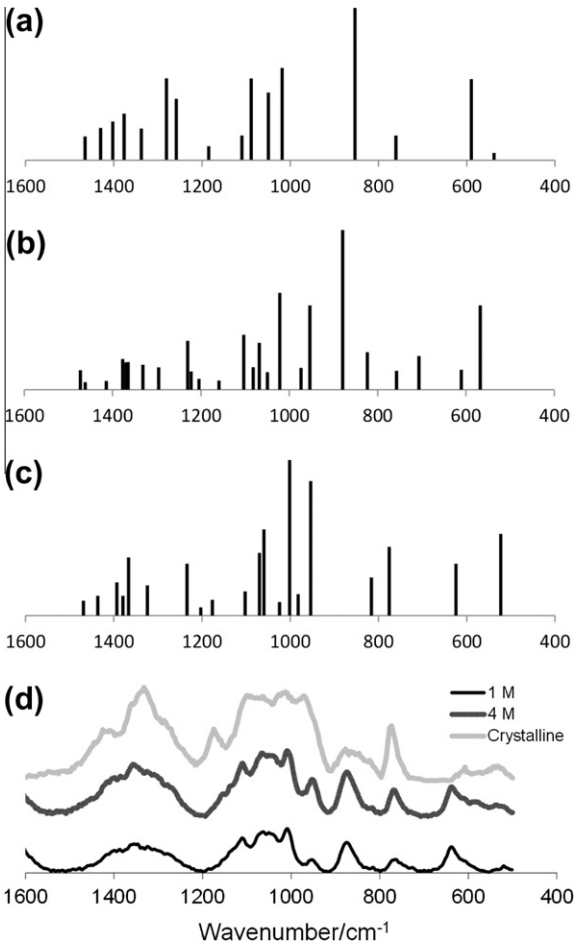

Fig. 5. Comparison of calculated and experimental Raman spectra of glyoxal derivatives: (a) calculated monomer dihydrate, (b) calculated glyoxal dimer dihydrate, (c) calculated glyoxal trimer dihydrate, and (d) experimental spectra of glyoxal 1 and 4 M solutions and crystalline glyoxal trimer dihydrate.

The calculated wavenumber for νC—C stretching of dihydrated glyoxal monomer is 853 cm^{-1}. This mode involves strong degree of δOH bending. The linear νC—C of hydrated glyoxal dimer (hemiacetal-ring link) is predicted to arise at 879 cm^{-1} (Table 1). For the deuterated glyoxal monomer hydrate, the νC—C theoretical wavenumber is shifted to 793 cm^{-1}, indicating that C—C stretching and OD bending vibrations are coupled. Theoretical wavenumber for the linear νC—C of deuterated glyoxal dimer is 859 cm^{-1} (Table 2). The band at 865 cm^{-1} in the theoretical spectra of deuterated glyoxal monomer is assigned to νC—O vibration mixed with δOD. Because of strong coupling, no individual vibration corresponding to the νC—C linkage between two dioxolane rings appears in the calculated spectra of glyoxal trimer dihydrate or its deuterated analogue.

Barker et al. identified the strong peak at 830 cm^{-1} as the stretching of methyl-ring in highly polarized methyl substituted 1,3-dioxolanes [36]. In another study, the Raman spectrum of single crystals of oxalic acid dihydrate contained showed medium to strong peaks at 865 and 855 cm^{-1} which were attributed to C—C stretching vibrations [38]. For the deuterated analogue, this bands shifted to 844–845 cm^{-1} and the intensities increased. The same authors attributed the medium-strong band at 844 cm^{-1} to out-of-plane OH bending (γOH) associated with water libration. In deuterated oxalic acid dihydrate samples, the γOH bending band appears at 812 cm^{-1} [38]. In addition, Plath and Axson report a theoretical IR peak at 843 cm^{-1} due to νC—C coupling with δOH and a second peak at 759 cm^{-1} due to a decoupling C—C stretching of glyoxylic acid monohydrate [33]. According to calculation and literature data, we attribute the band at 872 cm^{-1} to a νC—C of dihydrated glyoxal monomer coupling with δOH with a possible minor contribution of linear νC—C of dihydrated glyoxal dimer.

Region 800–700 cm^{-1}. A broad band at 762 cm^{-1} is observed in the spectra of glyoxal solutions in H_2O and D_2O (Fig. 3). The band shape arises due to multiple transitions. We assigned this band to the O—C—O bending of dehydrated glyoxal monomer on the basis of a theoretical value of 761 cm^{-1} for in-plane O—C—O bending vibration (Table 1). Upon drying, the band at 762 cm^{-1} shifted to a higher wavenumber of 770 cm^{-1} and increased in intensity. Since the predicted wavenumber for the O—C—O ring bending in glyoxal trimer is 775 cm^{-1}, we attribute the band at 770 cm^{-1} to O—C—O bending of 5-member dioxolan ring of glyoxal oligomers.

In the work by Loeffler et al. [10] FTIR has been used to investigate equilibria between different forms of hydrated glyoxal in evaporating droplets, but no theoretical confirmation of the spectral peak assignments has been provided. To fill this gap, we collected infrared spectra of aqueous glyoxal solutions and made peak assignments with the aid of theoretically calculated vibrational wavenumbers and insight from the Raman spectra. Fig. 4 shows FTIR spectra of 1–4 M glyoxal solutions obtained in our study. The spectrum of 1 M glyoxal solution features a strong band at 1070 cm^{-1} with a shape suggesting that the band contains several overlapping transitions. The calculated wavenumbers for νC—O are 1050, 1088 and 1110 cm^{-1} for the dihydrated glyoxal monomer (Table 1). For the dihydrated glyoxal dimer the calcu-

lated IR wavenumbers are 1050 and 1080 cm^{-1}. According to calculations, we assigned this group of bands in IR spectra to a νC—O coupled with δCOH dihydrated glyoxal monomer, with a possible contribution from the dihydrated glyoxal dimer. The spectrum of 1 M glyoxal solution also has low intensity peaks of at 1009 and 950 cm^{-1}. In the spectrum of 4 M glyoxal solution, the band at 1070 cm^{-1} overlaps with a strong absorption at 1050 cm^{-1}, corresponding to νC—O of the dihydrated glyoxal dimer. The bands at 1009 and 950 cm^{-1} are more prominent in the spectrum of the more concentrated solution. Our calculations predict a peak at 947 cm^{-1} due to in-plane stretching of glyoxal trimer active in IR. The observed IR absorbance at 950 cm^{-1} has been attributed to an asymmetrical C—O—C stretching of 5-membered dioxolane ring.

Since the formation of acetals involves the interaction of a carbonyl with an OH group, glyoxal monohydrate plays a central role in oligomerization of glyoxal in aqueous solutions [10,14]. The equilibrium concentration of the monohydrate depends on the water activity and is expected to increase upon droplet evaporation. Since the stretching wavenumber of the carbonyl C=O groups in Raman and IR spectra (1620–1800 cm^{-1}) is overlapped by a strong O—H scissoring bend of liquid H_2O at 1640 cm^{-1}, monitoring the evolution of carbonyl in aqueous solutions is challenging. On the contrary, in deuterated water solutions, the O–D scissoring bend of liquid D_2O is shifted to 1200 cm^{-1} and the behavior of the carbonyl can be monitored unobstructed. By conducting experiments in D_2O, we find that the carbonyl feature at 1600–1800 cm^{-1} is not observable in 1 M glyoxal solution. Furthermore, it does not appear upon evaporation, when the equilibrium of Reaction (1) is shifted to higher wavenumbers, thus suggesting that in aqueous solutions glyoxal exists predominantly in dihydrated form. This is in agreement with findings of Malik and Joens [39], who observed that less than 0.02% of the glyoxal molecules in aqueous solution exist in the free dialdehyde form, 1.98% of the molecules exist in monoaldehyde form, and approximately 98% of the molecules are hydrated at both carbonyl groups.

Conclusions

Experimental Raman and IR spectra of glyoxal solutions of various concentrations were obtained and peak assignments were made with the aid of DFT calculations. Interpretation of spectra is challenging, because several forms of glyoxal derivatives with similar functional groups, e.g., hydroxyl and dioxolane ring, are present in glyoxal solutions. Furthermore, the degree of coupling between different vibrations is high in the compounds studied and few of the modes arise from a single type of molecular vibration.

In the Raman spectra of aqueous glyoxal solutions, the presence of bands corresponding to deformation vibrations of the dioxolane ring was observed in solutions with glyoxal concentrations in the range from 1 M and above indicating the presence of dihydrated glyoxal dimer oligomers. Upon evaporation of the solution, oligomers are transformed to dihydrate glyoxal trimer. The absence of a detectable signal of a carbonyl group in 1–4 M aqueous glyoxal solutions indicates that the equilibrium concentration of the monohydrated form remains low even in evaporating droplets.

Under typical ambient temperature and humidity conditions, evaporation of glyoxal solutions resulted in incomplete water loss. The presence of residual water was confirmed using Raman spectra. Our results suggest that the formation of crystalline trimer from relatively concentrated (>0.5 M) droplets is hindered by the high viscosity of amorphous trimer and requires extremely dry conditions that could be hardly achieved in the atmosphere. Hence, in the atmosphere particles containing these organic compounds may be present in an amorphous state under a broad range of conditions. In addition, the Raman and IR peak assignments determined in this study by combining experimental measurements and theoretical calculations will be useful in future applications, including heterogeneous chemistry of glyoxal in cloud droplets.

Acknowledgement

The authors gratefully acknowledge financial support for this research from Robert Welch Foundation.

Appendix A. Supplementary material

Supplementary data associated with this article can be found, in the online version, at http://dx.doi.org/10.1016/j.saa.2012.09.050.

References

[1] M. Kalberer, D. Paulsen, M. Sax, M. Steinbacher, J. Dommen, A.S.H. Prevot, R. Fisseha, E. Weingartner, V. Frankevich, R. Zenobi, U. Baltensperger, Identification of polymers as major components of atmospheric organic aerosols, Science 303 (2004) 1659–1662.
[2] Y. Tan, A.G. Carlton, S.P. Seitzinger, B.J. Turpin, SOA from methylglyoxal in clouds and wet aerosols: measurement and prediction of key products, Atmos Environ 44 (2010) 5218–5226.
[3] R.Y. Zhang, I. Suh, J. Zhao, D. Zhang, E.C. Fortner, X.X. Tie, L.T. Molina, M.J. Molina, Atmospheric new particle formation enhanced by organic acids, Science 304 (2004) 1487–1490.
[4] R. Volkamer, F.S. Martini, L.T. Molina, D. Salcedo, J.L. Jimenez, M.J. Molina, A missing sink for gas-phase glyoxal in Mexico City: formation of secondary organic aerosol, Geophys Res Lett (2007) 34.
[5] T. Koop, J. Bookhold, M. Shiraiwa, U. Poschl, Glass transition and phase state of organic compounds: dependency on molecular properties and implications for secondary organic aerosols in the atmosphere, Phys. Chem. Chem. Phys. 13 (2011) 19238–19255.
[6] X. Zhou, K. Mopper, Apparent partition coefficients of 15 carbonyl compounds between air and sea water and between air and freshwater; implications for air-sea exchange, Environ. Sci. Technol. 24 (1990) 1864–1869.
[7] P. Warneck, Multi-phase chemistry of C2 and C3 organic compounds in the marine atmosphere, J. Atmos. Chem. 51 (2005) 119–159.
[8] B. Noziere, A. Cordova, A kinetic and mechanistic study of the amino acid catalyzed aldol condensation of acetaldehyde in aqueous and salt solutions, J. Phys. Chem. A 112 (2008) 2827–2837.
[9] B. Noziere, P. Dziedzic, A. Cordova, Products and kinetics of the liquid-phase reaction of glyoxal catalyzed by ammonium ions (NH(4)(+)), J. Phys. Chem. A 113 (2009) 231–237.
[10] K.W. Loeffler, C.A. Koehler, N.M. Paul, D.O. De Haan, Oligomer formation in evaporating aqueous glyoxal and methyl glyoxal solutions, Environ. Sci. Technol. 40 (2006) 6318–6323.
[11] E.B. Whipple, Structure of glyoxal in water, J. Am. Chem. Soc. 92 (1970) 7183. - &.
[12] F. Chastrette, C. Bracoud, M. Chastrette, G. Mattioda, Y. Christidis, Study of aqueous glyoxylic-acid solutions by C-13 NMR, Bull. Soc. Chim. France (1985) 66–74.
[13] F. Chastrette, M. Chastrette, C. Bracoud, Acetalization of aqueous glyoxal solution – structure determination by tandem gas-chromatography – mass-spectrometry and factorial analysis, Bull. Soc. Chim. France (1986) 822–836.
[14] J. Kua, S.W. Hanley, D.O. De Haan, Thermodynamics and kinetics of glyoxal dimer formation: a computational study, J. Phys. Chem. A 112 (2008) 66–72.
[15] W.P. Hastings, C.A. Koehler, E.L. Bailey, D.O. De Haan, Secondary organic aerosol formation by glyoxal hydration and oligomer formation: humidity effects and equilibrium shifts during analysis, Environ. Sci. Technol. 39 (2005) 8728–8735.
[16] J.L. Axson, K. Takahashi, D.O. De Haan, V. Vaida, Gas-phase water-mediated equilibrium between methylglyoxal and its geminal diol, Proc. Nat. Acad. Sci. USA 107 (2010) 6687–6692.
[17] C. Marcolli, B.P. Luo, T. Peter, F.G. Wienhold, Internal mixing of the organic aerosol by gas phase diffusion of semivolatile organic compounds, Atmos. Chem. Phys. 4 (2004) 2593–2599.
[18] L. Wang, W. Xu, A.F. Khalizov, J. Zheng, C. Qiu, R.Y. Zhang, Laboratory investigation on the role of organics in atmospheric nanoparticle growth, J. Phys. Chem. A 115 (2011) 8940–8947.
[19] L.K. Kho, V.I. Tyulin, Raman-spectrum of liquid glyoxal $C_2O_2H_2$, Opt. Spektrosk. 35 (1973) 770–772.
[20] A.R.H. Cole, J.R. Durig, Raman and infrared-spectra of solid glyoxal-D1 and glyoxal-D2, J. Raman Spectrosc. 4 (1975) 31–39.
[21] F. Verderam, E. Castellu, S. Califano, Infrared and Raman spectra of polycrystalline glyoxal, J. Chem. Phys. 52 (1970) 719.
[22] A.B. Duval, D.A. King, R. Haines, N.R. Isenor, B.J. Orr, Coherent Raman-spectroscopy of glyoxal vapor, J. Raman Spectrosc. 17 (1986) 177–182.

[23] M.J. Frisch, G.W. Trucks, H.B. Schlegel, G.E. Scuseria, M.A. Robb, J.R. Cheeseman, J.A. Montgomery Jr., T. Vreven, K.N. Kudin, J.C. Burant, J.M. Millam, S.S. Iyengar, J. Tomasi, V. Barone, B. Mennucci, M. Cossi, G. Scalmani, N. Rega, G.A. Petersson, H. Nakatsuji, M. Hada, M. Ehara, K. Toyota, R. Fukuda, J. Hasegawa, M. Ishida, T. Nakajima, Y. Honda, O. Kitao, H. Nakai, M. Klene, X. Li, J.E. Knox, H.P. Hratchian, J.B. Cross, C. Adamo, J. Jaramillo, R. Gomperts, R.E. Stratmann, O. Yazyev, A.J. Austin, R. Cammi, C. Pomelli, J.W. Ochterski, P.Y. Ayala, K. Morokuma, G.A. Voth, P. Salvador, J.J. Dannenberg, V.G. Zakrzewski, S. Dapprich, A.D. Daniels, M.C. Strain, O. Farkas, D.K. Malick, A.D. Rabuck, K. Raghavachari, J.B. Foresman, J.V. Ortiz, Q. Cui, A.G. Baboul, S. Clifford, J. Cioslowski, B.B. Stefanov, G. Liu, A. Liashenko, P. Piskorz, I. Komaromi, R.L. Martin, D.J. Fox, T. Keith, M.A. Al-Laham, C. Y. Peng, A. Nanayakkara, M. Challacombe, P.M.W. Gill, B. Johnson, W. Chen, M.W. Wong, C. Gonzalez, J.A. Pople, Gaussian Inc., Wallingford, CT, 2004.
[24] F. Jensen, Introduction to Computational Chemistry, second ed., Wiley, 2006.
[25] D. Michalska, R. Wysokinski, The prediction of Raman spectra of platinum(II) anticancer drugs by density functional theory, Chem. Phys. Lett. 403 (2005) 211–217.
[26] D. Rappoport, F. Furche, Lagrangian approach to molecular vibrational Raman intensities using time-dependent hybrid density functional theory, J. Chem. Phys. 126 (2007).
[27] J.R. Cheeseman, M.J. Frisch, Basis set dependence of vibrational Raman and Raman optical activity intensities, J. Chem. Theory Comput. 7 (2011) 3323–3334.
[28] Y. Marechal, Infrared-spectra of water. 1. Effect of temperature and of H/D isotopic dilution, J. Chem. Phys. 95 (1991) 5565–5573.
[29] G. Socrates, Infrared and Raman characteristic Group frequencies: tables and charts, third ed., John Wiley & Sons, Chichester, 2001.
[30] L.J. Bellamy, The infrared spectra of complex molecules, third ed., John Wiley & Sons, New York, 1975.
[31] J. Murto, A. Kivinen, K. Edelmann, E. Hassinen, Fluoroalcohols. 21. Infrared, matrix infrared and Raman-spectra of 1,1,1-trifluoro-2-propanol and its three deuterated analogs, Spectroc. Acta Pt. A-Molec. Biomolec. Spectr. A 31 (1975) 479–493.
[32] D.M.W. Anderson, L.J. Bellamy, R.L. Williams, The infrared spectra of some gem dihydroxy compounds and their deuterated derivatives, Spectrochim. Acta 12 (1958) 233–238.
[33] K.L. Plath, J.L. Axson, G.C. Nelson, K. Takahashi, R.T. Skodje, V. Vaida, Gas-phase vibrational spectra of glyoxylic acid and its gem diol monohydrate, Implications for atmospheric chemistry, reaction kinetics and catalysis letters 96 (2009) 209–224.
[34] G. Cassanas, M. Morssli, E. Fabregue, L. Bardet, Vibrational-spectra of lactic-acid and lactates, J. Raman Spectrosc. 22 (1991) 409–413.
[35] S.A. Barker, E.J. Bourne, R.M. Pinkard, D.H. Whiffen, Spectra of acetals. 1. The infrared and Raman spectra of 1-3-dioxolan, J. Chem. Soc. (1959) 802–806.
[36] S.A. Barker, E.J. Bourne, R.M. Pinkard, D.H. Whiffen, Spectra of acetals. 2. The infrared and raman spectra of substituted 1-3-dioxolans, J. Chem. Soc. (1959) 807–813.
[37] J.R. Quinan, S.E. Wiberley, Infrared and Raman spectra of a series of deuterated alcohols, Anal. Chem. 26 (1954) 1762–1764.
[38] V. Mohacek-Grosev, J. Grdadolnik, J. Stare, D. Hadzi, Identification of hydrogen bond modes in polarized Raman spectra of single crystals of alpha-oxalic acid dihydrate (vol 40, pg 1605, 2009), J. Raman Spectrosc. 41 (2010) 598.
[39] M. Malik, J.A. Joens, Temperature dependent near-UV molar absorptivities of glyoxal and gluteraldehyde in aqueous solution, Spectroc. Acta Pt. A-Molec. Biomolec. Spectr. 56 (2000) 2653–2658.